Solvent-assisted control of metal-organic nanotube size and morphology

Nathan D. Rosenmann¹, Jacob A. Barrett², Shengyi Su³, Nathan C. Gianneschi^{1,3,4*},

David M. Jenkins^{2*}

- ¹ Department of Materials Science and Engineering, International Institute for Nanotechnology, Chemistry of Life Processes Institute, Simpson Querrey Institute, Northwestern University, Evanston, IL 60208, USA
- ² Department of Chemistry, University of Tennessee, Knoxville, TN 37996, USA
- ³ Department of Chemistry, International Institute for Nanotechnology, Chemistry of Life Processes Institute, Simpson Querrey Institute, Northwestern University, Evanston, IL 60208, USA
- ⁴Department of Biomedical Engineering, Northwestern University, Evanston IL, 60208, USA
- * nathan.gianneschi@northwestern.edu
- * jenkins@ion.chem.utk.edu

ABSTRACT: While intensive studies have focused on the synthesis and characterization of new metal organic nanotube (MONT) structures, the lack of size and morphology control remains an obstacle in broadening applications for this class of materials. Herein, we demonstrate control of MONT crystallite size and morphology by tuning polarity and the protic/aprotic nature of solvents, including dimethylformamide (DMF), N-methyl-2-pyrrolidone (NMP), ethanol (EtOH), or 2-methyltetrahydrofuran (MeTHF), for the isostructural syntheses of two MONTs. Through a combination of transmission electron microscopy (TEM), powder X-ray diffraction (PXRD), and selected area electron diffraction (SAED), we find that MONT crystallite sizes can be tuned while maintaining control over relative dispersity without significantly altering the underlying crystal structure.

Introduction

Metal-organic nanotubes (MONTs) are materials that share similar tunability and porosity to their 3-dimensional counterpart, metal-organic frameworks (MOFs).^{1, 2} Like MOFs, MONTs are typically synthesized by ordered assembly of organic linkers and inorganic metal salts.² MONTs have been shown to be amenable to applications which exploit their porosity, including gas storage and liquid separation.³⁻⁶ Previous studies on MONTs have not only focused on controlling the pore shape and aperture through modular approaches (e.g. 2-pillar, 4-pillar, and 6-pillar), but also expanded towards multivariate ligand functionality to successfully generate a statistically copolymerized MONT.⁷⁻¹²

Yet, a key aspect of MONT tunability that has yet to be fully explored is the ability to control the size and morphology of the synthesized crystallites. It has been previously demonstrated

that the utilization of different solvents for MOF synthesis can result in a change in crystal size and morphology, where previous works have demonstrated that even subtle changes to the solvothermal MOF synthesis (i.e., solvent ratios or exchanging solvents) resulted in significant changes in crystallite morphology and size.¹³⁻¹⁵ In some cases, these changes could result in variations in porosity and adsorption capabilities.^{16, 17} While there have been considerable efforts in exploring this aspect within the field of MOFs through a variety of methods, including temperature control, addition of surfactants, solvents selection, and a variety of other methods, there is limited research in showing the same can be accomplished for MONTs.¹⁸⁻²³

Typically, as-synthesized MONT structures are solved and refined by single crystal X-ray diffraction (SCXRD), yet this technique is typically limited to large (> 20 microns), high-quality crystals to produce atomically precise structures. Thus, it is highly likely that there are MONT structures that have been missed by most common methods due to their nanoscale morphology (<500 nm diameter). To further investigate and confirm the generation of nanoscale MONTs and MOFs, we must rely heavily on a combination of powder X-ray diffraction (PXRD), transmission electron microscopy (TEM), and selected area electron diffraction (SAED) to properly characterize the crystal structure and morphology of nanoscale MONT crystals.

As a proof of concept, we report the first size and morphology control of MONT structures using different solvents in their syntheses. We have chosen to investigate two previously reported MONTs and examine how the use of different organic solvents resulted in the different size of the yielded MONTs, as previous works have demonstrated that using similar solvents for MOF synthesis resulted in changed morphology.^{13, 14, 16} Here, we focus on the reactions of (4,4'-(1,4-(2,3,5,6-tetrafluoroxylene)-diyl)bis(1,2,4-triazole) ligand (L1) and 1,4-bis((4H-1,2,4-triazol-4-yl)methyl)naphthalene ligand (L2) with copper(II) bromide to generate crystalline MONTs in dimethylformamide (DMF), N-methyl-2-pyrrolidone (NMP), 2-methyltetrahydrofuran (MeTHF), and ethanol (EtOH) (Figure 1).^{7,24} TEM images revealed that crystal size and morphology of the two systems varied significantly from reactions using different solvents, resulting in a reduction in crystallite size of three orders of magnitude by using EtOH rather than DMF without significant changes in relative size dispersity. The crystal structures remained mostly unchanged, as evidenced by the alignments of PXRD patterns and well-matched lattice parameters from SAED.

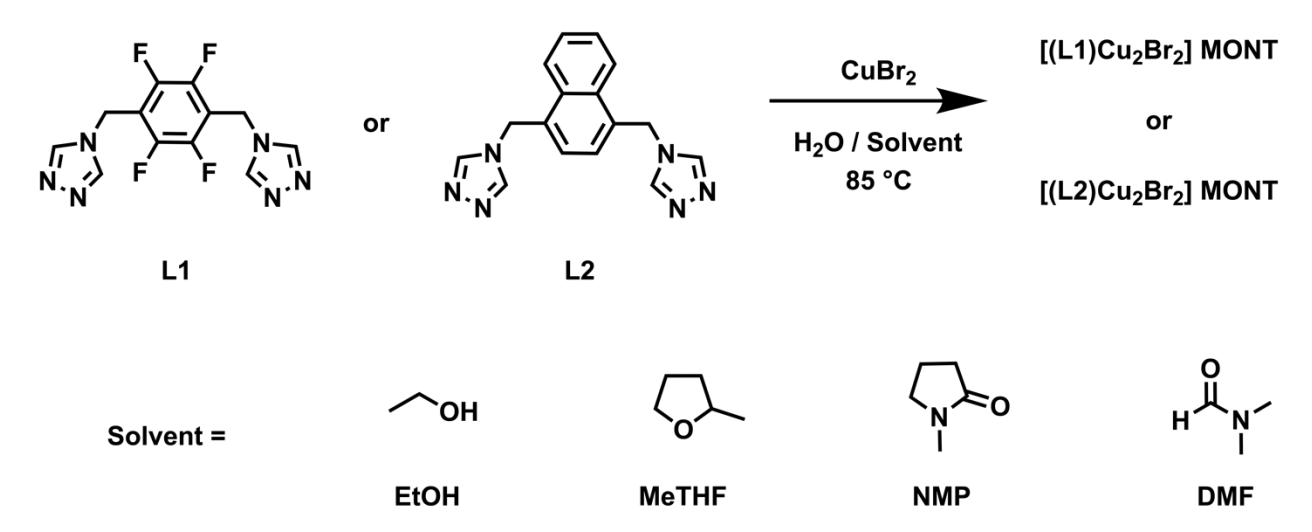


Figure 1. MONT reaction scheme.

Results and Discussion

L1, **L2**, [(**L1**)Cu₂Br₂] MONTs, and [(**L2**)Cu₂Br₂] MONTs were synthesized following previously reported procedures with slight modifications.^{7, 24} Briefly, reactions were performed at 85 °C of a 1:2 mixture of copper(II) bromide dissolved in water and the ligand dissolved in an amide solvent such as DMF, where the reactions achieve completion within seven days as the copper is reduced to a copper(I) species and the crystallites no longer noticeably grow any further.

Conventional solvents for MONT formation typically include DMF or NMP – where these solvents are polar aprotic in nature. Meanwhile, MOF literature has suggested that the addition of polar protic solvents, such as water or EtOH, alter crystallite size and morphology due to hydrogen bonding between the ligand and solvent in the presence of anionic species. ^{25, 26} We hypothesized that crystal growth could be driven by both the nature of the solvent and the solubility of the ligand, where decreased ligand solubility and increased hydrogen bonding between the ligand and the polar protic solvent will increase the nucleation rate and result in many nanoscale crystallites rather than the previously reported macroscale MONT crystallites. ¹⁵ Thus, we predicted the replacement of DMF with NMP would still result in the growth of macroscale crystallites, while utilizing EtOH or MeTHF would result in nanoscale crystallites. We note that although MeTHF displays some polar aprotic nature, we predict that its immiscibility with water should produce MONT crystals that are smaller than those produced with DMF but larger than those produced with EtOH. Notably, while both ligands are soluble in DMF and NMP, the ligands require sonication to become soluble in most other solvents.

To monitor the generation of crystallites and examine their size and morphology, we prepared diluted samples for examination via TEM following the reaction reaching completion after seven days at 85 °C. The images were then analyzed to determine the average value and polydispersity of their size and aspect ratio (**Figure 2** and **Figure 3**). The crystal structures of the resulting precipitates were subsequently examined via SAED

(**Figure S1** and **Figure S2**). Following washing and drying, the remaining bulk product was then analyzed via PXRD. If the resulting crystals were large enough, the crystals were also characterized via SCXRD.

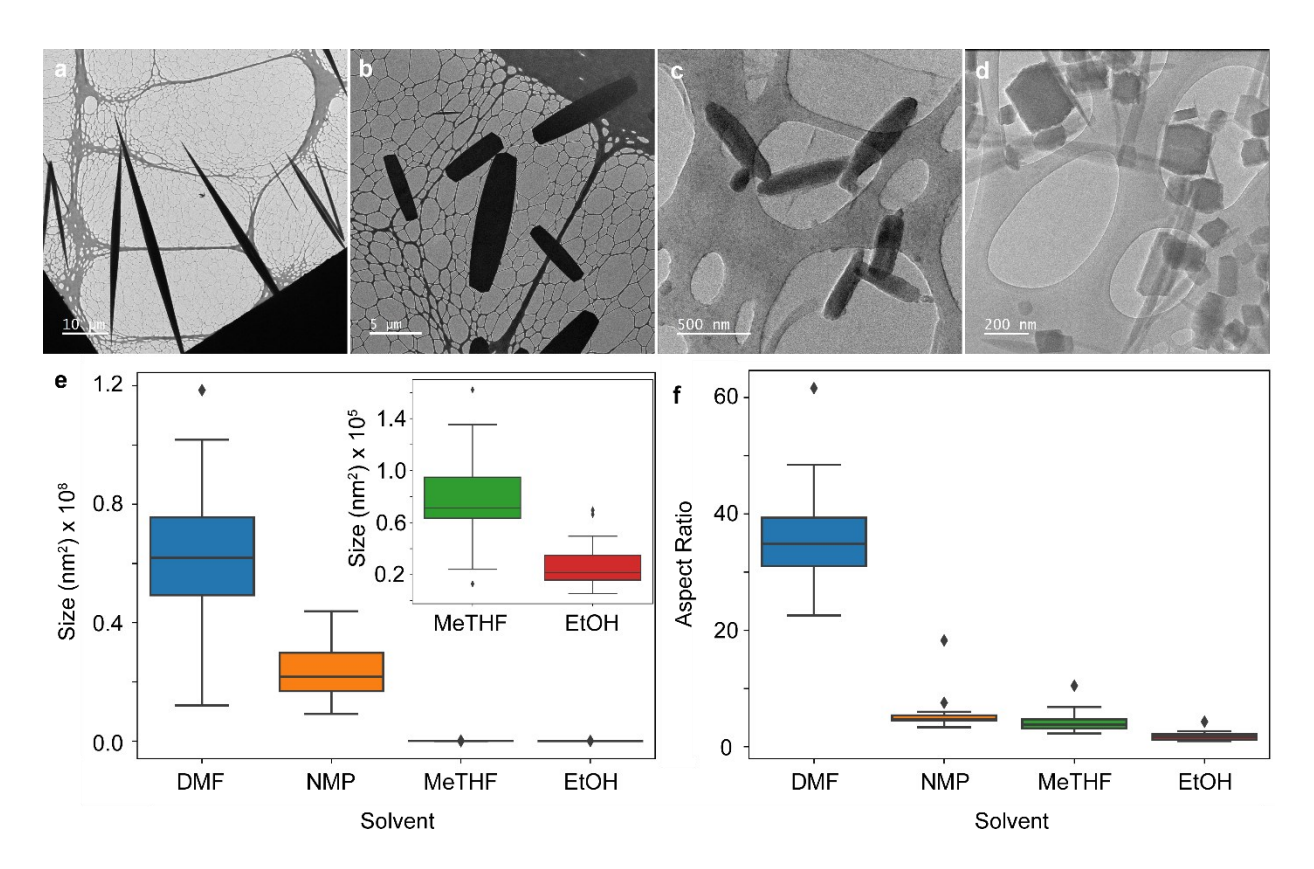


Figure 2. a-d. TEM of [(**L1**)Cu₂Br₂] MONTs produced in DMF, NMP, MeTHF, and EtOH after 7 days, respectively. **e-f.** Distribution of size and aspect ratio [(**L1**)Cu₂Br₂] MONTs resulting from TEM image analysis.

Solvent	Size (nm²)	σ _{Size} (nm ²)	Aspect Ratio	σ AspectRatio
DMF	6.14E+07	2.55E+07	35.46	7.66
NMP	2.37E+07	1.01E+07	5.23	2.34
MeTHF	7.64E+04	3.34E+04	4.16	1.58
EtOH	2.69E+04	1.71E+04	1.77	0.68

Table 1. Size, aspect ratio, and respective standard deviations found by image analysis of TEM of [(L1)Cu₂Br₂] MONT produced in DMF, NMP, MeTHF, and EtOH after 7 days.

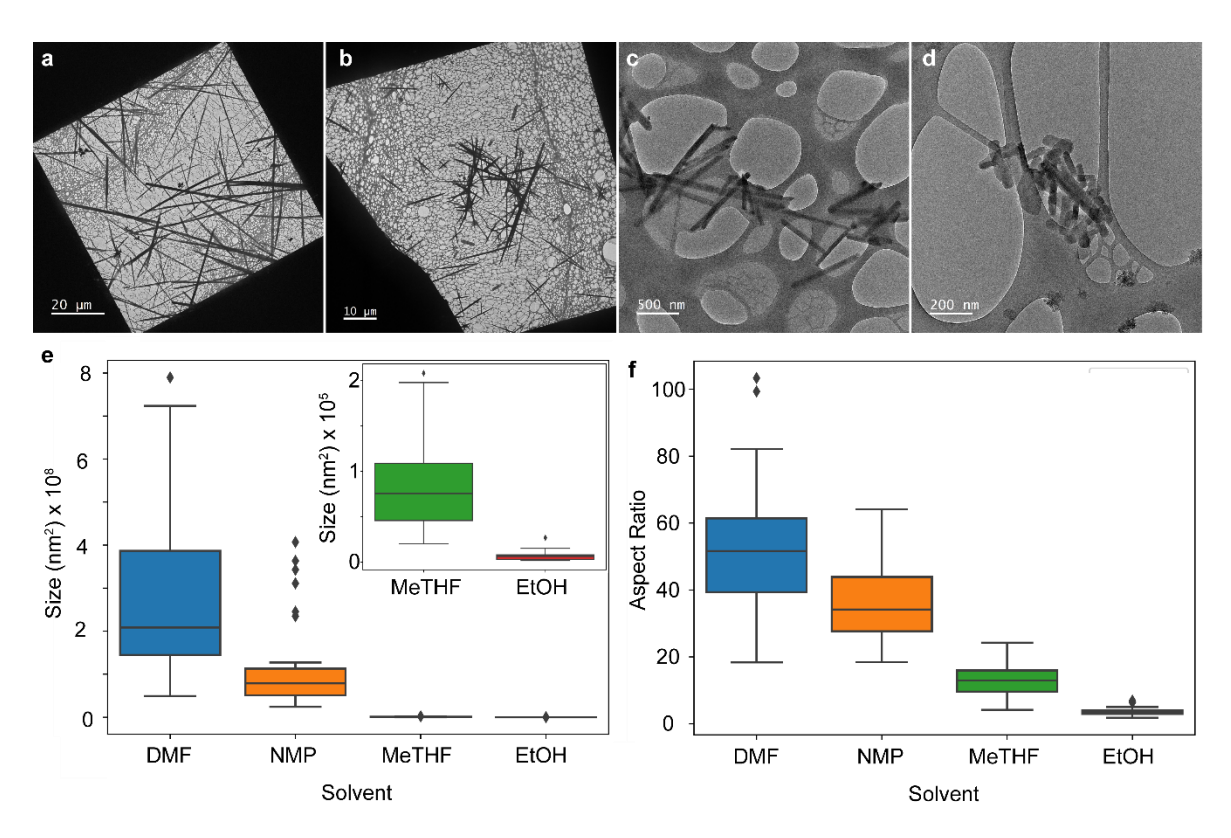


Figure 3. a-d. TEM of [(**L2**)Cu₂Br₂] MONTs produced in DMF, NMP, MeTHF, and EtOH after 7 days, respectively. **e-f**. Distribution of size and aspect ratio [(**L2**)Cu₂Br₂] MONTs resulting from TEM image analysis.

Solvent	Size (nm²)	σ_{Size} (nm ²)	Aspect Ratio	σ AspectRatio
DMF	2.78E+07	1.93E+07	53.03	19.53
NMP	1.18E+07	1.06E+07	36.91	12.33
MeTHF	8.36E+04	4.79E+04	13.20	5.06
EtOH	4.39E+03	2.08E+03	3.54	1.09

Table 2. Table including size, aspect ratio, and respective standard deviations found by image analysis of TEM of [(**L2**)Cu₂Br₂] MONT produced in DMF, NMP, MeTHF, and EtOH after 7 days.

TEM micrographs of [(L1)Cu₂Br₂] MONTs reveal a difference between crystallite size among those synthesized with DMF, NMP, MeTHF, and EtOH (Figure 2a-2d). Notably, MONTs synthesized in DMF exhibited an average crystallite size three orders of magnitude greater than the MONTs synthesized with EtOH (Figure 2e and Table 2). We also note the decrease in the crystallite aspect ratio with decreasing crystallite size (Figure 2f). We believe this change is caused by the inability of the crystals to grow beyond their nucleation seed. Thus, the crystallites possess a parallelepiped morphology when formed in EtOH rather than rod-

like when formed in DMF or NMP. A similar trend was observed for the [(**L2**)Cu₂Br₂] MONTs synthesized with DMF, NMP, MeTHF, and EtOH (**Figure 3a-3f** and **Table 2**).

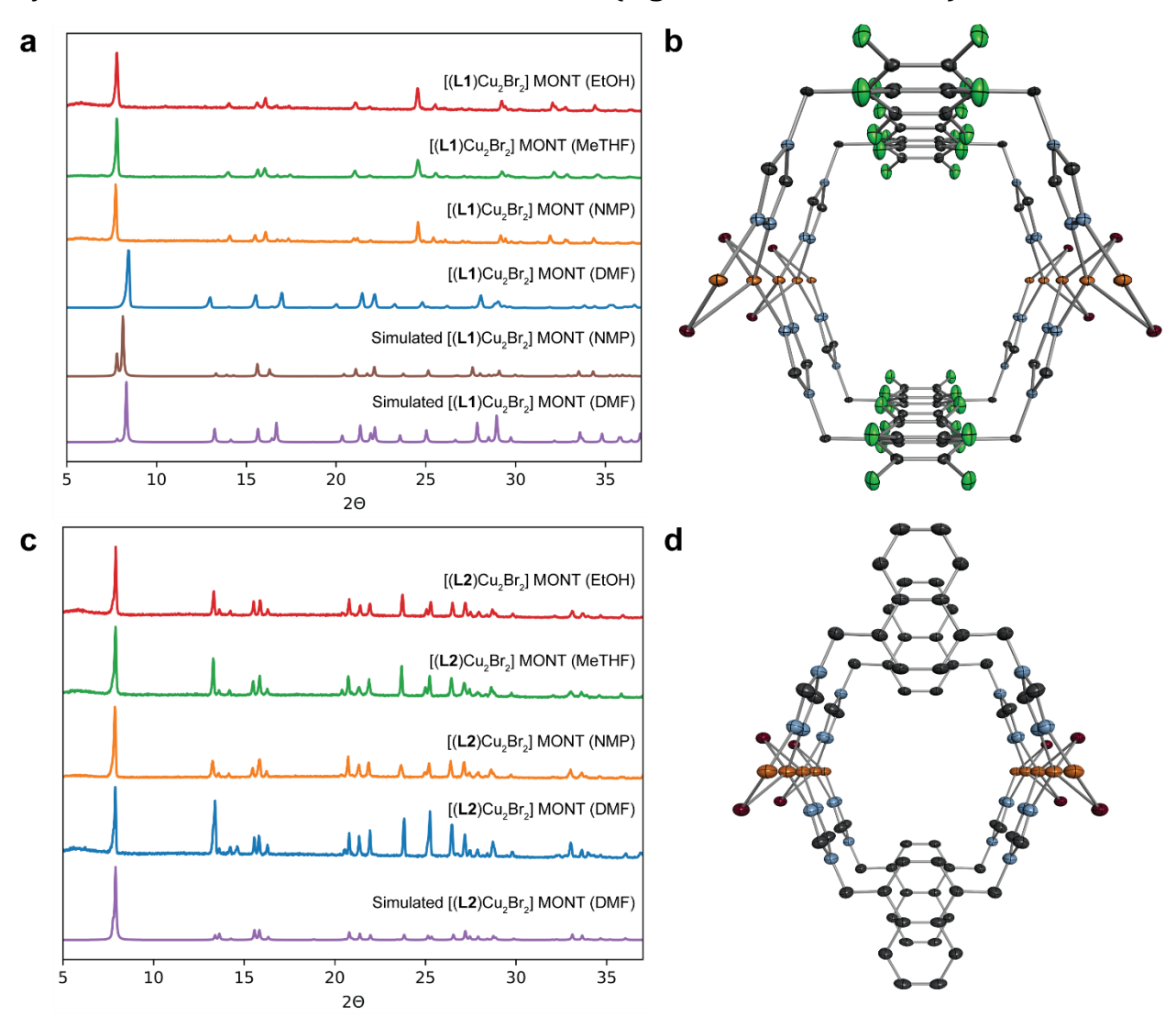


Figure 4. a. PXRD of [(**L1**)Cu₂Br₂] MONTs depicting identical diffraction patterns between MONTs produced in different solvents. We note the diffraction patterns are quite similar to the simulated and previously published PXRD. **b.** SCXRD of [(**L1**)Cu₂Br₂] MONT synthesized in DMF. **c.** PXRD of [(**L2**)Cu₂Br₂] MONTs depicting identical diffraction patterns between MONTs produced in different solvents. We note the diffraction patterns are quite similar to the simulated and previously published PXRD. **d.** SCXRD of [(**L2**)Cu₂Br₂] MONT synthesized in DMF

The resulting MONTs were also characterized by X-ray diffraction to confirm that all MONTs shared an identical crystal structure irrespective of solvent (**Figure 4**). The PXRD patterns generated for all [(**L1**)Cu₂Br₂] MONTs and [(**L2**)Cu₂Br₂] MONTs match simulated and previously published MONTs from DMF and diethylformamide, respectively (**Figure 4a** and

4c).^{7, 24} SCXRD was performed on MONT crystals if they were sufficiently large, and we confirmed that the PXRD for [(**L1**)Cu₂Br₂] MONTs synthesized in DMF and [(**L2**)Cu₂Br₂] MONTs synthesized in NMP match the previously published structures (**Figure 4b** and **4d**).^{7, 24} The PXRD patterns of [(**L1**)Cu₂Br₂] synthesized in DMF and in NMP are not identical to each other due to subtle changes of the unit cell parameters as a result of the tilt of the tetrafluorinated phenyl moiety. The phenyl moiety tilts significantly more in NMP than DMF (21° compared to 16° via SCXRD) and results in a larger crystallographic a-axis. This leads to a shift to smaller 2θ in the PXRD for hkl values where h ≠0. Notably, the naphthyl ring cannot rotate in [(**L2**)Cu₂Br₂] due to π - π stacking. As this feature is absent from [(**L2**)Cu₂Br₂] MONTs, nearly identical PXRD patterns are observed despite changes in organic solvent. Additional SCXRD data can be found in the SI (**Figure S4-5** and **Table S3**).

Due to the size of the EtOH and MeTHF MONT crystallites (<500 nm), it is not feasible to determine an exact crystal structure via standard SCXRD setups. Using SCXRD data, we can simulate electron diffraction patterns that correspond to the expected MONT crystal structures. Based on these simulated patterns and newly acquired SCXRD and PXRD, SAED confirms the generation of the expected MONT crystal structures (**Figure S1-S2**).

The change in size and morphology demonstrates a clear solvent effect in MONT synthesis similar to what has been previously observed in MOF synthesis. ^{13-15, 17, 25} It has been previously demonstrated that when using NMP to synthesize MONTs, the rate limiting step is nucleation – meaning that crystal growth dominates the kinetics of MONT formation. ²⁷ The sharp difference in the aspect ratios of [(L1)Cu₂Br₂] MONT structures generated by DMF and NMP (Table 1) indicate there is a significant change in the kinetics of MONT growth, as opposed to the gradual decrease in aspect ratio of L2 MONTs. Due to the high number of nanoscale MONTs produced in EtOH (Figure 2d and Figure 3d), we believe that the polar protic nature of EtOH has shifted the reaction kinetics to enhance nucleation. The enhanced nucleation of MONTs resulting from the use of MeTHF and EtOH as synthesis solvents results in numerous nanoscale crystallites that do not display any significant increase in size, suggesting that most of the reactants have been consumed during nucleation. After seven days, the [(L1)Cu₂Br₂] MONTs synthesized in DMF have grown substantially while the [(L1)Cu₂Br₂] MONTs synthesized in EtOH have displayed negligible growth (Figure S3a, and Figure S3b).

Conclusions

From the above results, we provide considerable evidence that size and morphology control of isostructural MONTs can be achieved using different solvents. The MONTs synthesized displayed a size change of up to three orders of magnitude, as well as a morphological change from a rod-like to parallelepiped structures, while maintaining identical crystal structures at the atomic scale. We aim to continue to investigate the versatility of these findings and will further understand the influence of size and morphology on the properties of MONTs (i.e., porosity, adsorption capability, catalytic activity).

Author Contributions

N.D.R. performed nanoscale and bulk MONT reactions and characterization via TEM and SAED. J.A.B. performed ligand synthesis and characterization of bulk MONT reactions via SCXRD. S.S. performed PXRD on bulk MONTs and aided in experimental setup. N.C.G. and D.M.J. designed and supervised the project. The manuscript was written by N.C.G., D.M.J., N.D.R., J.A.B., and S.S. and with input from all authors. The Table of Contents (TOC) figure was produced by J.A.B.

Supporting Information: The Supporting Information is available free of charge. Experimental details, SAED, TEM, and single crystal X-ray data are included as a PDF.

X-ray CIF files have been posted with the CCDC under the following numbers: 2325205 and 2325206. These contain the same materials grown under different solvent conditions.

Acknowledgements

J.A.B. and D.M.J. thank the National Science Foundation (NSF DMR-2207224) and the University of Tennessee for support. N.D.R., S.S., and N.C.G. thank the National Science Foundation (NSF DMR-2207269) for support. This work made use of the EPIC facility of Northwestern University's NUANCE Center, which has received support from the Soft and Hybrid Nanotechnology Experimental (ShyNE) Resource (NSF ECCS-1542205), the MRSEC program (NSF DMR-1720139) at the Materials Research Center, the International Institute for nanotechnology (IIN), the Keck Foundation, and the State of Illinois, through the IIN. N.D.R and S.S. also gratefully acknowledge the support from the Ryan Fellowship and the IIN at Northwestern University.

References

- (1) Wang, Q.; Astruc, D. State of the Art and Prospects in Metal-Organic Framework (MOF)-Based and MOF-Derived Nanocatalysis. *Chem Rev* **2020**, *120* (2), 1438-1511. DOI: 10.1021/acs.chemrev.9b00223 From NLM PubMed-not-MEDLINE.
- (2) Jia, J.-G.; Zheng, L.-M. Metal-organic nanotubes: Designs, structures and functions. *Coordination Chemistry Reviews* **2020**, *403*. DOI: 10.1016/j.ccr.2019.213083.
- (3) Fangna Dai, H. H., and Daofeng Sun. A Metal-Organic Nanotube Exhibiting Reversible Adsorption of (H2O)12 Cluster *JACS Communications* **2008**, *130* (43), 2.
- (4) Jia, J. G.; Feng, J. S.; Huang, X. D.; Bao, S. S.; Zheng, L. M. Homochiral iron(ii)-based metalorganic nanotubes: metamagnetism and selective nitric oxide adsorption in a confined channel. *Chem Commun (Camb)* **2019**, *55* (19), 2825-2828. DOI: 10.1039/c9cc00506d.
- (5) Zhou, Y.; Yao, S.; Ma, Y.; Li, G.; Huo, Q.; Liu, Y. An anionic single-walled metal-organic nanotube with an armchair (3,3) topology as an extremely smart adsorbent for the effective and selective adsorption of cationic carcinogenic dyes. *Chem Commun (Camb)* **2018**, *54* (24), 3006-3009. DOI: 10.1039/c8cc00542g.
- (6) Unruh, D. K.; Gojdas, K.; Libo, A.; Forbes, T. Z. Development of metal-organic nanotubes exhibiting low-temperature, reversible exchange of confined "ice channels". *J Am Chem Soc* **2013**, *135* (20), 7398-7401. DOI: 10.1021/ja400303f.
- (7) Barrett, J. A.; Rosenmann, N. D.; Gnanasekaran, K.; Carroll, X. B.; Gianneschi, N. C.; Jenkins, D. M. Statistical copolymer metal organic nanotubes. *Chem Sci* **2023**, *14* (4), 1003-1009. DOI: 10.1039/d2sc06084a.
- (8) Ding, B.; Guo, C.; Liu, S. X.; Cheng, Y.; Wu, X. X.; Su, X. M.; Liu, Y. Y.; Li, Y. A unique multifunctional cationic luminescent metal–organic nanotube for highly sensitive detection of dichromate and selective high capacity adsorption of Congo red. *RSC Advances* **2016**, *6* (40), 33888-33900. DOI: 10.1039/c6ra03576k.
- (9) Lv, L.-L.; Zhang, L.-J.; Zhao, H.; Wu, B.-L. Syntheses, structures and properties of nickel(II) and manganese(II) coordination polymers based on V-shaped bis-imidazole and aromatic carboxylate ligands. *Polyhedron* **2016**, *115*, 204-211. DOI: 10.1016/j.poly.2016.05.019.
- (10) Otake, K.; Otsubo, K.; Sugimoto, K.; Fujiwara, A.; Kitagawa, H. Ultrafine Metal-Organic Right Square Prism Shaped Nanowires. *Angew Chem Int Ed Engl* **2016**, *55* (22), 6448-6451. DOI: 10.1002/anie.201601678 From NLM PubMed-not-MEDLINE.
- (11) Yang, X.-K.; Chang, M.-N.; Hsing, J.-F.; Wu, M.-L.; Yang, C.-T.; Hsu, C.-H.; Chen, J.-D. Synthesis, crystal structures and thermal properties of six Co(II) and Ni(II) coordination polymers with mixed ligands: Formation of a quadruple-strained helical nanotube. *Journal of Molecular Structure* **2018**, *1171*, 340-348. DOI: 10.1016/j.molstruc.2018.06.036.
- (12) Murdock, C. R.; Jenkins, D. M. Isostructural synthesis of porous metal-organic nanotubes. *J Am Chem Soc* **2014**, *136* (31), 10983-10988. DOI: 10.1021/ja5042226 From NLM PubMed-not-MEDLINE.
- (13) Sanil, E. S.; Cho, K.-H.; Lee, S.-K.; Lee, U. H.; Ryu, S. G.; Lee, H. W.; Chang, J.-S.; Hwang, Y. K. Size and morphological control of a metal–organic framework Cu-BTC by variation of solvent and modulator. *Journal of Porous Materials* **2014**, *22* (1), 171-178. DOI: 10.1007/s10934-014-9883-7.

- (14) Bustamante, E. L.; Fernandez, J. L.; Zamaro, J. M. Influence of the solvent in the synthesis of zeolitic imidazolate framework-8 (ZIF-8) nanocrystals at room temperature. *J Colloid Interface Sci* **2014**, *424*, 37-43. DOI: 10.1016/j.jcis.2014.03.014.
- (15) Sun, J.; Yu, X.; Zhao, S.; Chen, H.; Tao, K.; Han, L. Solvent-Controlled Morphology of Amino-Functionalized Bimetal Metal-Organic Frameworks for Asymmetric Supercapacitors. *Inorg Chem* **2020**, *59* (16), 11385-11395. DOI: 10.1021/acs.inorgchem.0c01157.
- (16) Yang, J.-M.; Liu, Q.; Sun, W.-Y. Shape and size control and gas adsorption of Ni(II)-doped MOF-5 nano/microcrystals. *Microporous and Mesoporous Materials* **2014**, *190*, 26-31. DOI: 10.1016/j.micromeso.2014.01.020.
- (17) Akhundzadeh Tezerjani, A.; Halladj, R.; Askari, S. Different view of solvent effect on the synthesis methods of zeolitic imidazolate framework-8 to tuning the crystal structure and properties. *RSC Adv* **2021**, *11* (32), 19914-19923. DOI: 10.1039/d1ra02856a.
- (18) Luczak, J.; Kroczewska, M.; Baluk, M.; Sowik, J.; Mazierski, P.; Zaleska-Medynska, A. Morphology control through the synthesis of metal-organic frameworks. *Adv Colloid Interface Sci* **2023**, *314*, 102864. DOI: 10.1016/j.cis.2023.102864.
- (19) Zhao, J.; Liu, X.; Wu, Y.; Li, D.-S.; Zhang, Q. Surfactants as promising media in the field of metal-organic frameworks. *Coordination Chemistry Reviews* **2019**, *391*, 30-43. DOI: 10.1016/j.ccr.2019.04.002.
- (20) Seoane, B.; Dikhtiarenko, A.; Mayoral, A.; Tellez, C.; Coronas, J.; Kapteijn, F.; Gascon, J. Metal organic framework synthesis in the presence of surfactants: towards hierarchical MOFs? *CrystEngComm* **2015**, *17* (7), 1693-1700. DOI: 10.1039/c4ce02324b.
- (21) Feng, L.; Wang, K.-Y.; Powell, J.; Zhou, H.-C. Controllable Synthesis of Metal-Organic Frameworks and Their Hierarchical Assemblies. *Matter* **2019**, *1* (4), 801-824. DOI: 10.1016/j.matt.2019.08.022.
- (22) Kim, K. J.; Li, Y. J.; Kreider, P. B.; Chang, C. H.; Wannenmacher, N.; Thallapally, P. K.; Ahn, H. G. High-rate synthesis of Cu-BTC metal-organic frameworks. *Chem Commun (Camb)* **2013**, 49 (98), 11518-11520. DOI: 10.1039/c3cc46049e.
- (23) Sarawade, P.; Tan, H.; Anjum, D.; Cha, D.; Polshettiwar, V. Size- and shape-controlled synthesis of hexagonal bipyramidal crystals and hollow self-assembled Al-MOF spheres. *ChemSusChem* **2014**, *7* (2), 529-535. DOI: 10.1002/cssc.201300836 From NLM Medline.
- (24) Vailonis, K. M.; Gnanasekaran, K.; Powers, X. B.; Gianneschi, N. C.; Jenkins, D. M. Elucidating the Growth of Metal-Organic Nanotubes Combining Isoreticular Synthesis with Liquid-Cell Transmission Electron Microscopy. *J Am Chem Soc* **2019**, *141* (26), 10177-10182. DOI: 10.1021/jacs.9b04586.
- (25) Israr, F.; Chun, D.; Kim, Y.; Kim, D. K. High yield synthesis of Ni-BTC metal-organic framework with ultrasonic irradiation: Role of polar aprotic DMF solvent. *Ultrason Sonochem* **2016**, *31*, 93-101. DOI: 10.1016/j.ultsonch.2015.12.007 From NLM PubMed-not-MEDLINE.
- (26) Usman, K. A. S.; Maina, J. W.; Seyedin, S.; Conato, M. T.; Payawan, L. M.; Dumée, L. F.; Razal, J. M. Downsizing metal-organic frameworks by bottom-up and top-down methods. *NPG Asia Materials* **2020**, *12* (1). DOI: 10.1038/s41427-020-00240-5.
- (27) Etampawala, T.; Mull, D. L.; Keum, J. K.; Jenkins, D. M.; Dadmun, M. Insights into the Morphology and Kinetics of Growth of Silver Metal-Organic Nanotubes. *Crystal Growth & Design* **2016**, *16* (3), 1395-1403. DOI: 10.1021/acs.cgd.5b01509.